Visualizing Spin-Dependent Electronic Collisions In Ferromagnets

S. N. Samarin, J. Berakdar,* O. Artamonov, and J. Kirschner

Max-Planck-Institut für Mikrostrukturphysik, Weinberg 2, 06120 Halle, Germany

This work demonstrates experimentally and theoretically that the coincident two-electron emission from a ferromagnetic surface, upon the impact of a polarized electron, carries detailed information on the spin-dependent electronic collisions in ferromagnets. The analysis of the calculated and the measured two-electron spectra reveals the potential of the electron-pair emission technique for the study of (a) surface magnetism and (b) spin-dependent electron scattering dynamics in ferromagnets.

Magnetic systems with reduced dimensionality, such as ultrathin ferromagnetic films and magnetic surfaces are in the focus of current experimental and theoretical investigations [1,2]. These studies are driven by the fundamental importance of such materials and by their technological potential for magnetic storage and recording media as well as by the prospects of the fabrication of artificially synthesized devices. A number of dynamical features of magnetic systems are primarily controlled by the spin-dependent excitation spectrum [2]. Examples of such properties are the response characteristics and the spin dependence of the mean-free path of excited electrons. Thus, experimental techniques that probe the spin-dependent excitation of magnetic systems are of considerable value. One of the established methods that serves this purpose is the spin polarized electron energy loss spectroscopy (SPEELS). As low energy electrons can penetrate only the first few atomic layers, SPEELS can be employed to investigate the elementary excitations of magnetic systems with reduced symmetry [3]. For example, the Stoner spectrum (electron hole pair spectrum) has been successfully explored by SPEELS [4,5]. The Stoner excitation involves, at least, a two state transition: A majority band electron interacts with an incoming polarized electron (of opposite spin projection) and goes over into a vacuum state. Upon this interaction, the projectile electron loses energy and occupies an empty state in the minority band. This collision process is called exchange scattering. In SPEELS only one (the excited majority band electron) of the two participating electronic states is resolved. Obviously, valuable details of the exchange scattering dynamics are obscured by averaging over the second electron not detected by SPEELS. Therefore, we designed an experiment which measures the two-electron coincident emission rate from a magnetic surface following the impact of a polarized electron, while the energies (E_1, E_2) and the emission angles of the two emitted electrons as well as the energy E_0 and the angle of incidence of the electron beam are being determined (cf. Fig. 1). Hence, the wave vectors $\mathbf{k}_0$ and $\mathbf{k}_1, \mathbf{k}_2$ of the impinging and two receding electrons are measured in coincidence. The escaping electrons are detected using two time of flight

(TOF) detectors [6]. The sample normal, the incident electron beam, and the axes of the TOF detectors are chosen to be in the same plane. The polarization vector $\mathbf{P}_e$ of the incident beam and the magnetization direction of the sample, a bcc Fe(110) single crystal, are both perpendicular to the scattering plane (cf. Fig. 1). As a source of spin polarized electrons we used a strained GaAs multilayer photocathode activated by Cs deposition and oxygen exposure. Photoelectrons generated from the photocathode by the circularly polarized light of the laser diode were deflected by a 90° deflector to convert the longitudinally polarized beam into a transversely polarized one. The average count rate of coincidence was 1 event per second. For reasonable statistics a typical spectrum takes an acquisition time of about 270 hours. This long term measurement requires the stability of electronics, constant incident current, and good vacuum conditions. To reduce the influence of the possible instabilities the polarization of the incident beam is inverted every 5 seconds and the data for each polarization are stored in two different files. In spite of the UHV conditions ($\approx 5 \times 10^{-11}$ mbar) the cleanliness of the sample surface has to be ensured regularly (by Ar^+ ion sputtering followed by an annealing and, if necessary, oxygen treatment to remove the carbon from the surface). The surface properties were monitored
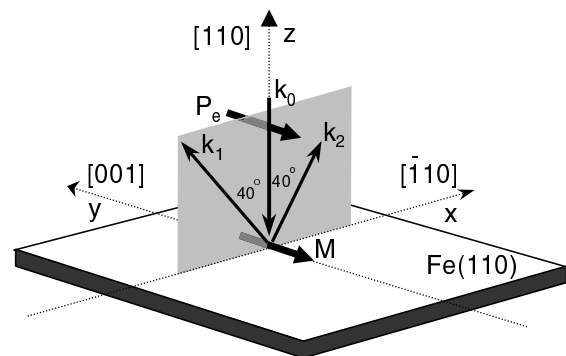

FIG. 1. The experimental setup as used for the coincident measurements. The direction of the magnetization $\mathbf{M}$, the spin polarization vector of the incoming beam $\mathbf{P}_e$ as well as the wave vectors of the incoming and the two emitted electrons $\mathbf{k}_0$ and $\mathbf{k}_1$ and $\mathbf{k}_2$ are indicated. The electron detectors are positioned at 40° to the left and to the right of the z axis.

    0031-9007/00/85(8)/1746(4)$15.00

using Auger electron spectroscopy and low-energy electron diffraction. The experiment requires a high degree of polarization of the incident beam and a single domain magnetization of the sample. To guarantee that these conditions are given we employed SPEELS and measured the energy loss spectra (the Stoner spectrum) for an electron beam polarization parallel and antiparallel to the magnetization in the same geometry of Fig. 1 while one of the TOFs is being switched off. The asymmetry A, derived from the two intensities for the opposite spin projections of the incident beam, is measured before and after the coincidence experiments and is used as an indicator for the stability of the experimental setup.

As illustrated in Figs. 1 and 2, the energy and wave vector balance impose the conditions

$$E_0 + \epsilon = E_1 + E_2, \tag{1}$$

$$\mathbf{k}_{0,\parallel} + \mathbf{q}_\parallel + \mathbf{g}_\parallel = \mathbf{k}_{1,\parallel} + \mathbf{k}_{2,\parallel}. \tag{2}$$

Here, ϵ is the energy of the valence band electron and $\mathbf{q}_\parallel$ is its (surface) Bloch wave vector. The surface reciprocal lattice vector is denoted by $\mathbf{g}_\parallel$. Since the quantities E_0, E_1, E_2 and $\mathbf{k}_0, \mathbf{k}_{1,\parallel}, \mathbf{k}_{2,\parallel}$ are determined experimentally [cf. Figs. 1 and 2] we can control, via Eqs. (1) and (2), the values of ϵ and $\mathbf{q}_\parallel$; i.e., we can perform the experiment in a certain region of the (magnetic) surface Brillioun zone. For example, by lowering E_2 while keeping E_1 and E_0 fixed we can zoom in deeper levels of conduction band [cf. Figs. 2(a) and 2(b)]. Equivalently, one can scan $\mathbf{q}_\parallel$ by varying, e.g., $\mathbf{k}_{0,\parallel}$ for given $\mathbf{k}_{1,\parallel}$, $\mathbf{k}_{2,\parallel}$, and $\mathbf{g}_\parallel$.

The role of the exchange scattering in the present experiment is illustrated in Figs. 2(a)–2(d). In the reaction shown in Fig. 2(a) the impinging electron escapes as the fast electron, i.e., $E_1 > E_2$. This process is called the direct scattering and proceeds with an amplitude f. In contrast, as illustrated in Fig. 2(c), the incoming electron may *exchange* as much energy and momentum with the initially bound one that it emerges as the slower one ($E_1 < E_2$). This scattering process is precisely the one active in the case of the aforementioned Stoner excitation. It is usually referred to as the exchange process and is

quantified with an amplitude g. Intuitively one can expect that $|f| \gg |g|$ for $E_0 \approx E_1$ and $E_1 \gg E_2 \ll E_0$.

Our experiment does not resolve the electron spin projections in the final state, i.e., we cannot distinguish between the processes shown in Figs. 2(a) and 2(c). Thus, the coincident rate for antiparallel [Fig. 2(a)] or parallel [Fig. 2(b)] alignment of the spins of the incoming and the bound electron is proportional to $|f|^2 + |g|^2$ and $|f - g|^2$, respectively. This is because the processes shown in Figs. 2(a) and 2(c) can be distinguished experimentally while the processes shown in Figs. 2(b) and 2(d) are experimentally identical, and hence f and g are added coherently. Theoretically, to sum over the (final-state) spin quantum numbers we couple the electrons' spins to the (conserved) total spin of the electron pair S and end up with two spin channels: the singlet channel ($S = 0$) and the triplet channel ($S = 1$). The singlet (triplet) cross section $X^{(S=0)}$ ($X^{(S=1)}$) can then be expressed in terms of f and g [7]. The experiment (Fig. 1) measures a spin asymmetry $\mathcal{A}$; i.e., for a certain magnetization direction $\mathbf{M}$, we register the electron-pair emission rate W for antiparallel [$W(\downarrow\uparrow)$] and parallel [$W(\uparrow\uparrow)$] alignment of the polarization vector of the incoming beam with $\mathbf{M}$ (cf. Fig. 1) and evaluate $\mathcal{A}$ as

$$\mathcal{A}(\mathbf{k}_1, \mathbf{k}_2; \mathbf{k}_0) = \frac{W(\downarrow\uparrow) - W(\uparrow\uparrow)}{W(\downarrow\uparrow) + W(\uparrow\uparrow)}. \tag{3}$$

For a gaseous atomic target with a defined spin polarization P_a (taken as a quantization axis) the asymmetry $\mathcal{A}$ is directly expressible in terms of $X^{(S=0/1)}$ (and hence in terms of f and g) as [7] $\mathcal{A} = P_a P_e A^{(s)}$, $A^{(s)} = (X^{(S=0)} - X^{(X=1)})/(X^{(S=0)} + 3X^{(S=1)}) = (2|f| \times |g| \cos\delta)/(|f|^2 + |g|^2 + |f + g|^2)$, where δ is the phase difference between the amplitudes f and g. This relation for $\mathcal{A}$ implies that $\lim_{(|g|/|f|)\to 0} A \to 0$, as discussed and shown experimentally below. For magnetized surfaces, the spin polarization of electronic states is dependent on the binding energy ϵ and on $\mathbf{q}_\parallel$; i.e., the theory has to consider the spin resolved Bloch spectral functions w rather then the density of states. The influence
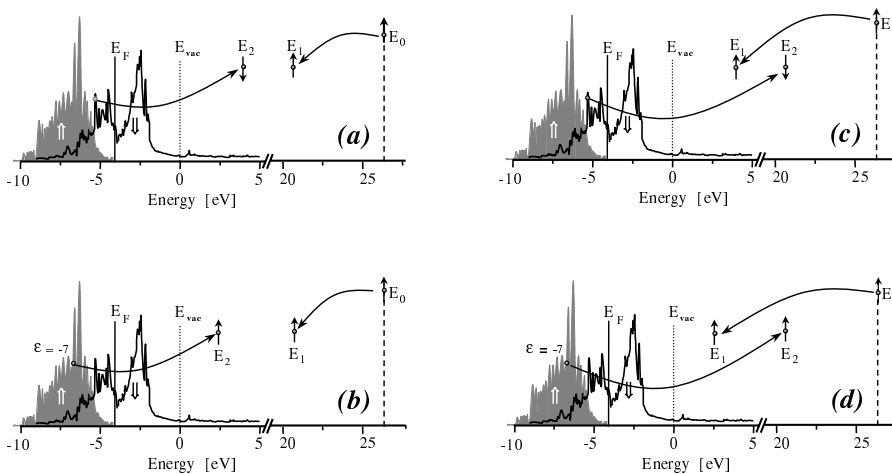

FIG. 2. An illustration of the direct (a),(b) and the exchange (c),(d) scattering (see text for details). The energies of the incoming and the two escaping electrons are denoted by E_0 and E_1, E_2. The vacuum and the Fermi levels are shown as E_{vac} and E_F. ϵ is the initial binding energy of the ejected electron. The surface density of states of the majority band (referred to by $\Uparrow$) and the minority band (indicated by $\Downarrow$) are shown.

of the crystal structure on the scattering dynamics is encompassed in f and g. The *exchange* induced asymmetry $\mathcal{A}$ has the form [8] (other spin asymmetries [8] are negligible within the accuracy of the present experiment)

$$\mathcal{A}(\mathbf{k}_1, \mathbf{k}_2; \mathbf{k}_0) = P_e \frac{\sum_{l, \mathbf{g}_\parallel} A_l^{(m)} A_{l, \mathbf{g}_\parallel}^{(s)} \mathcal{B}_{l, \mathbf{g}_\parallel}}{\sum_{l', \mathbf{g}'_\parallel} \mathcal{B}_{l', \mathbf{g}'_\parallel}}. \quad (4)$$

Here, the atomic layers parallel to the surface are indexed by l. In Eq. (4) $A^{(m)}$ describes the *sample's magnetic asymmetry,* whereas the dynamical aspects of the spin-dependent collisions are contained in the *exchange scattering asymmetry* $A^{(s)}$. The spin averaged intensity is referred to as $\mathcal{B}$. This interpretation follows from the definitions of $A^{(m)}$, $A^{(s)}$, and $\mathcal{B}$

$$A_l^{(m)} = \frac{w(\mathbf{q}_\parallel, l, \epsilon, \Downarrow) - w(\mathbf{q}_\parallel, l, \epsilon, \Uparrow)}{w_0(\mathbf{q}_\parallel, l, \epsilon)}, \quad (5)$$

$$A_{l, \mathbf{g}_\parallel}^{(s)} = \frac{X^{(S=0)}(\mathbf{k}_1, \mathbf{k}_2; \mathbf{k}_0, \mathbf{g}_\parallel, l) - X^{(S=1)}(\mathbf{k}_1, \mathbf{k}_2; \mathbf{k}_0, \mathbf{g}_\parallel, l)}{3X^{(S=1)}(\mathbf{k}_1, \mathbf{k}_2; \mathbf{k}_0, \mathbf{g}_\parallel, l) + X^{(S=0)}(\mathbf{k}_1, \mathbf{k}_2; \mathbf{k}_0, \mathbf{g}_\parallel, l)}, \quad (6)$$

$$\mathcal{B}_{l, \mathbf{g}_\parallel} = w_0(\mathbf{q}_\parallel, l, \epsilon) \left[\frac{3}{4} X^{(S=1)} + \frac{1}{4} X^{(S=0)} \right], \quad (7)$$

where $w(\mathbf{q}_\parallel, l, \epsilon, \Uparrow)$ and $w(\mathbf{q}_\parallel, l, \epsilon, \Downarrow)$ are the Bloch spectral functions of, respectively, the majority and the minority bands. The spin averaged Bloch spectral function is w_0.

The calculational scheme for $A^{(m)}$, $A^{(s)}$, and $\mathcal{B}$ of Ref. [8] is employed for the subsequent numerical study. $A^{(m)}$ is derived from band structure calculations within the scalar relativistic full potential linearized augmented plane wave method [9], whereas $A^{(s)}$ and $\mathcal{B}$ are calculated from the layer dependent transition matrix elements.

Equations (5)–(7) demonstrate the versatile potential of the pair emission technique for material and scattering dynamics studies: (a) In case of unpolarized electrons and provided $X^{(S=1)}$ and $X^{(S=0)}$ are sufficiently known, the Bloch spectral functions w_0 can be mapped using Eq. (7). This is documented in Refs. [10,11] for diverse systems; (b) the magnetic asymmetry $A^{(m)}$ [i.e., Eq. (6)] in the spin-split band structure can be visualized by using polarized electron beam and choosing a geometrical arrangement under which the triplet channel is closed [8] ($X^{(S=1)} = 0$) in which case $A^{(s)} = 1$ [cf. Eq. (6)]; (c) conversely in the case that the spin polarized band structure is known, e.g., from reliable *ab initio* calculations, $A^{(m)}$ can be deduced from Eq. (5) and the spin scattering dynamics, which is embedded in $A^{(s)}$, can be extracted from the measured asymmetry $\mathcal{A}$ [Eq. (4)].

The present experimental setup does not yet allow one to explore in full detail all these facets of the pair emission technique. In particular, the averaging over the present angular resolution involves an integration over $\mathbf{q}_\parallel$ that extends basically over the entire surface Brillouin zone. The $\mathbf{q}_\parallel$ integration of the Bloch spectral functions [cf. Eq. (5)] yields the surface spin split density of states $\rho(\epsilon, \Uparrow), \rho(\epsilon, \Downarrow)$ that are depicted in Fig. 2. For the interpretation of the data we employ thus $A^{(m)} \approx [\rho(\epsilon, \Downarrow) - \rho(\epsilon, \Uparrow)]/[\rho(\epsilon, \Downarrow) + \rho(\epsilon, \Uparrow)]$.

In Figs. 3(a) and 3(b) the asymmetry $\mathcal{A}$ is scanned as a function of the energy sharing within the electron pair for a fixed total energy $E = E_1 + E_2$. According to Eq. (1) the energy of the valence band state ϵ is then fixed (E_0 is constant). When the two electrons escape with equal energies $E_1 = E_2$ the triplet scattering $X^{(S=1)}$ vanishes due to symmetry [8], and hence for $E_1 = E_2$ we obtain $A^{(s)} = 1$,

as experimentally verified in a recent work [7]. Therefore, in this situation ($E_1 = E_2$), the *magnitude* and *sign* of the asymmetry $\mathcal{A}$ are dictated merely by $A^{(m)}(\epsilon)$ which in Fig. 3(a) amounts to $A^{(m)}(\epsilon = -5.3 \text{ eV}) \approx +60\%$. This interpretation can be substantiated experimentally by shifting ϵ deeper into the band [cf. Figs. 2(a) and 2(b)] in which case $A^{(m)}$ changes sign. This results, as shown in Fig. 3(b) ($\epsilon = -7$ eV and $A^{(m)} \approx -40\%$), in an inverted sign of $\mathcal{A}$ as compared to the case of a positive $A^{(m)}$.
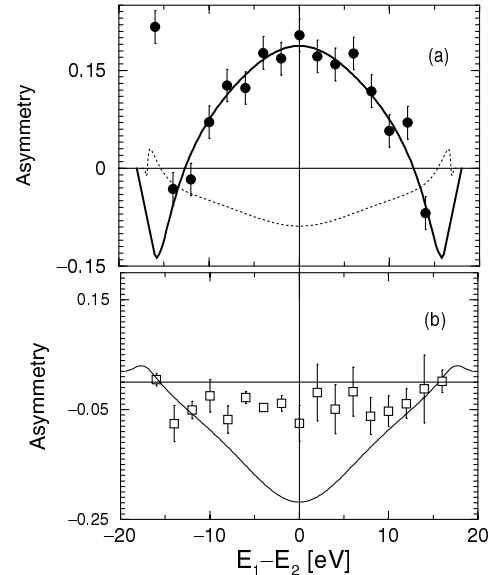

FIG. 3. (a) The measured (full dots) and calculated spin asymmetry $\mathcal{A}$ as a function of the energy sharing $E_1 - E_2$ for a fixed total energy $E = E_1 + E_2 = 17.7 \pm 0.7$ eV. The surface (bulk) electronic band structure has been employed for the calculations shown by the solid (dotted) line. The incident electron energy is $E_0 = 23$ eV; i.e., ϵ is just below E_F [cf. Fig. 2(a)]. The sample and the scattering geometry are as shown in Fig. 1. The theoretical results are averaged over the angular and the excess energy (E) resolution of the detectors. (b) The same as in (a) except that the energies are chosen as $E_0 = 26$ eV and $E = 19 \pm 1$ eV; i.e., ϵ is well below E_F [cf. Fig. 2(b)]. The experimental findings (open squares) are shown along with the (surface) calculations (solid curve).
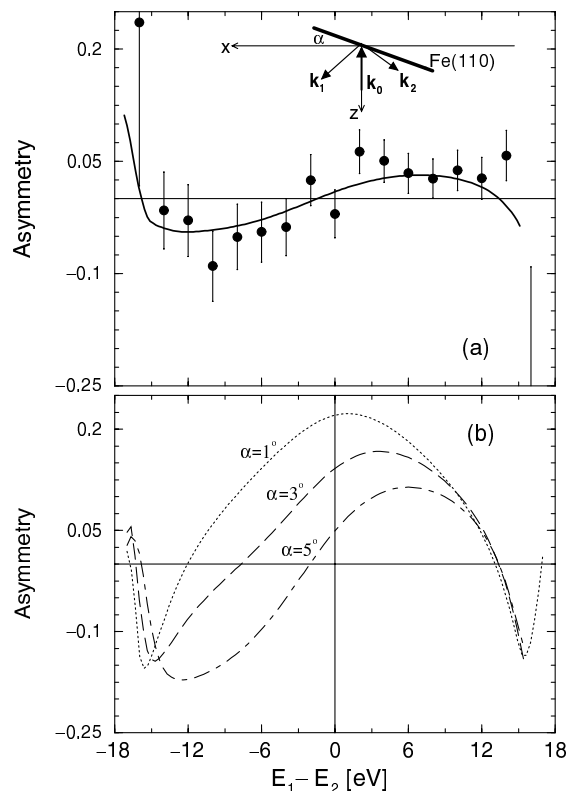
FIG. 4. (a) The measured (full dots) and calculated (solid curve) asymmetry for the same sample, incident, and excess energies as in Fig. 3(a) ($E_0 = 23$ eV, $E = 17.7 \pm 0.7$ eV); however, the sample is tilted with respect to the incident beam by an angle $\alpha = 5°$, as shown in the inset. The calculations (solid curve) are averaged over the angular and energy resolution of the experiment, as done in Fig. 3(a). (b) The same situation as in (a) but $\mathcal{A}$ is calculated for different angles α (from $\alpha = 1$ to $\alpha = 5°$, as depicted on the curves). The excess energy is $E = 18$ eV. The curves are averaged only over the angular resolution of the detectors.

Since ϵ is constant in Fig. 3(a) (and hence $A^{(m)}$ is constant) the variation of $\mathcal{A}$ is due to the spin-dependent scattering dynamics which is dictated by $A^{(s)}$. Thus the structure of $\mathcal{A}$, as depicted in Figs. 3(a) and 3(b), can be understood as follows: At $E_1 = E_2$ the triplet cross section vanishes in which case $A^{(s)}$ attains its highest value (unity). This structure is a peak (minimum) when $A^{(m)} > 0$ ($A^{(m)} < 0$). The decline in $\mathcal{A}$ for $E_1 > E_2$ or $E_2 < E_1$ is due to a dominance of the direct scattering amplitude $|f|$ [Fig. 2(a)] over the exchange one $|g|$ [Fig. 2(c)]; i.e., it is more likely for the fast incoming electron to escape as the fast electron than for it to lose almost its whole energy and emerge as the slower one. As deduced above $\lim_{(|g|/|f|) \to 0} A^{(s)} = (|f||g|\cos\delta)/(|f|^2|g|^2 + |f||g|\cos\delta) \to 0$, and hence the asymmetry in Figs. 3(a) and 3(b) decreases with increasing deviations from $E_1 = E_2$.

Figure 3(a) shows the asymmetry as calculated using a surface and a bulk electronic band structure. The model employing bulk spectral functions is clearly at variance with the data. This is comprehensible as in our experiment *two* low-energy electrons have to escape the surface and hence the surface sensitivity is increased as compared to SPEELS.

The special symmetry of the experimental arrangement depicted in Fig. 1 implies a symmetrical $\mathcal{A}$ with respect to $E_1 = E_2$ (in our case, spin orbit effects are negligibly small). This symmetry is broken by tilting the sample as shown in the inset of Fig. 4. Since ϵ is fixed, $A^{(m)}$ has a fixed constant value in Fig. 4. Therefore, the structure of $\mathcal{A}$ is related to that of $A^{(s)}$. To explore the origin of the shape of $\mathcal{A}$ in Fig. 4(a) we carried out numerical calculations [Fig. 4(b)] for varying angle of incidence, ranging from the symmetric case of Fig. 3(a) to that of Fig. 4(a) (in the single atom case $\mathcal{A}$ remains unchanged). As seen in Fig. 4(b), with increasing values of α, the broad peak in Fig. 3(a) at $E_1 = E_2$ diminishes to the small positive hump around $E_1 - E_2 \approx 8$ eV in Fig. 4(a). Its origin can still be related to a small triplet contribution. The negative dip in Fig. 3(a) at the left wing develops to the broad valley at $E_1 - E_2 \approx 12$ eV in Fig. 4(a). This trend illustrates the subtle dependence of the scattering dynamics on the propagation directions of the electrons through the surface.

The present Letter illustrates evidently that the utilization of the coincident two-electron emission technique renders possible a novel insight into the spin-dependent electronic scattering at surfaces. Future refinement of the present study will yield yet more precise information on the spin polarization $A^{(m)}$ of the surface electronic states in a well-defined region of the surface magnetic Brillouin zone.

*Corresponding author.
  Email address: jber@mpi-halle.de
[1] A. Hubert and R. Schäfer, *Magnetic Domains: The Analysis of Magnetic Microstructures* (Springer-Verlag, Berlin, 1998).
[2] *Ultrathin Magnetic Structures,* edited by B. Heinrich and J. A. C. Bland (Springer-Verlag, Heidelberg, 1994).
[3] *Polarized Electrons in Surface Physics,* edited by R. Feder (World Scientific, Singapore, 1985).
[4] J. Kirschner, D. Rebenstorff, and H. Ibach, Phys. Rev. Lett. **53**, 698 (1984).
[5] D. L. Abraham and H. Hopster, Phys. Rev. Lett. **62**, 1157 (1989).
[6] O. M. Artamonov, S. N. Samarin, and J. Kirschner, Appl. Phys. A **65**, 535 (1997).
[7] M. Streun, G. Baum, W. Blask, and J. Berakdar, Phys. Rev. A **59**, R4109 (1999).
[8] J. Berakdar, Phys. Rev. Lett. **83**, 5150 (1999).
[9] X. Qian and W. Hübner, Phys. Rev. B **60**, 16 192 (1999).
[10] I. E. McCarthy and E. Weigold, Rep. Prog. Phys. **54**, 789 (1991).
[11] A. S. Kheifets, S. Iacobucci, A. Ruoccoa, R. Camilloni, and G. Stefani, Phys. Rev. B **57**, 7380 (1998).